© 2021. Published by The Company of Biologists Ltd | Development (2021) 148, dev198788. doi:10.1242/dev.198788

RESEARCH ARTICLE

The 3′UTR of the *Drosophila* CPEB translation factor gene *orb2* plays a crucial role in spermatogenesis

Rudolf Gilmutdinov[1], Eugene N. Kozlov[1], Konstantin V. Yakovlev[1,2], Ludmila V. Olenina[3], Alexei A. Kotov[3], Justinn Barr[4], Mariya Zhukova[1], Paul Schedl[4,*] and Yulii V. Shidlovskii[1,5]

ABSTRACT

CPEB proteins are conserved translation regulators involved in multiple biological processes. One of these proteins in *Drosophila*, Orb2, is a principal player in spermatogenesis. It is required for meiosis and spermatid differentiation. During the later process, *orb2* mRNA and protein are localized within the developing spermatid. To evaluate the role of the *orb2* mRNA 3′UTR in spermatogenesis, we used the CRISPR/Cas9 system to generate a deletion of the *orb2* 3′UTR, *orb2*^{R}. This deletion disrupts the process of spermatid differentiation but has no apparent effect on meiosis. Differentiation abnormalities include defects in the initial polarization of the 64-cell spermatid cysts, mislocalization of mRNAs and proteins in the elongating spermatid tails, altered morphology of the elongating spermatid tails, and defects in the assembly of the individualization complex. These disruptions in differentiation appear to arise because *orb2* mRNA and protein are not properly localized within the 64-cell spermatid cyst.

KEY WORDS: CPEB, Orb2, 3′UTR, mRNA localization, Spermatogenesis

INTRODUCTION

Cytoplasmic polyadenylation element binding (CPEB) proteins are highly conserved translation factors. They interact with special cytoplasmic polyadenylation element (CPE) motifs in the 3′UTRs of target transcripts and can activate or repress their translation depending on the biological context (Ivshina et al., 2014; Khan et al., 2015). Vertebrates have four functionally distinct CPEB proteins – CPEB1, CPEB2, CPEB3 and CPEB4 – whereas flies have two, Orb and Orb2. CPEB proteins take part in a broad range of biological processes, including translational control of embryonic cell division (Kronja and Orr-Weaver, 2011), cellular senescence (Groppo and Richter, 2011), and the formation of synaptic plasticity underlying learning and long-term memory (Hervas et al., 2020; Kruttner et al., 2015). They also have important functions in oogenesis and spermatogenesis. In *Xenopus* oocytes, for example, the sequential activation of CPEB1 and CPEB4 helps to control egg maturation (Hochegger et al., 2001; Igea and Méndez, 2010; Kronja and Orr-Weaver, 2011; Richter, 2007; Sarkissian et al., 2004).

The two CPEB proteins in flies, Orb and Orb2, differ significantly in their N-terminal ends and have largely different activities. Orb is required in the female germline for the proper development of the egg chamber and regulates the translation of oocyte transcripts at multiple time points during this process. It is also expressed during the last stages of spermatogenesis in spermatids and in a subset of mushroom body neurons in the fly brain (Castagnetti and Ephrussi, 2003; Chang et al., 1999, 2001; Tan et al., 2001). In contrast, Orb2 is more widely expressed and plays important roles in somatic development and spermatogenesis. During embryonic development, Orb2 is expressed at high levels in the central and peripheral nervous system and functions as a fidelity factor in asymmetric cell division in these tissues and in muscle progenitor cells (Hafer et al., 2011). In the adult, it has been implicated in learning and memory (Hervas et al., 2016; Kruttner et al., 2012, 2015).

In addition to these activities, Orb2 has crucial functions during spermatogenesis, and *orb2* mRNA and protein expression levels in adults are highest in the testes. Two Orb2 protein isoforms are expressed in the testes: the 60-kDa Orb2A isoform and the 75-kDa Orb2B isoform, the latter being more abundant. The two proteins share a 542-amino acid C-terminal sequence that includes several polyQ and polyG amino acid stretches, two RRM-type RNA-binding domains, and a zinc-finger domain. However, they have unique N-terminal domains of 162 and 9 amino acids, respectively. The transcripts encoding the larger isoform have relatively long 3′UTRs (580-5791 nt) with multiple CPEs and CPE-like elements, whereas the transcript encoding the smaller isoform has a short 3′UTR (~400 nt) with no CPEs. The large isoform is essential for male fertility, whereas the smaller isoform is not (Xu et al., 2012).

Orb2 expression is not observed at the early stage of spermatogenesis. It is not expressed in the germline stem cells, and only a very low level of protein can be detected in the mitotic cysts. However, Orb2 expression is substantially upregulated after the 16-cell cysts are formed and the interconnected spermatocytes duplicate their DNA and begin to grow. At this stage as well as during the two meiotic divisions, Orb2 is cytoplasmic and is largely delocalized except puncta around the nuclear envelope (Xu et al., 2012). Once the spermatocytes have fully matured, they synchronously enter meiosis I, which is followed by meiosis II. At the end of meiosis, a cyst consisting of 64 interconnected spermatids with haploid nuclei is formed. The cells in the cyst remain undifferentiated during the meiotic divisions but start to differentiate as soon as meiosis is completed. One of the first steps is the reorganization and oriented polarization of the germ

[1]Department of Gene Expression Regulation in Development, Institute of Gene Biology, Russian Academy of Sciences, Moscow 119334, Russia. [2]Laboratory of Cytotechnology, A.V. Zhirmunsky National Scientific Center of Marine Biology, Far Eastern Branch of the Russian Academy of Sciences, Vladivostok 690041, Russia. [3]Department of Molecular Genetics of Cell, Institute of Molecular Genetics, National Research Centre Kurchatov Institute, Moscow 123182, Russia. [4]Department of Molecular Biology, Princeton University, Princeton, NJ 08544-1014, USA. [5]Department of Biology and General Genetics, I.M. Sechenov First Moscow State Medical University, Moscow 119048, Russia.

*Author for correspondence (pschedl@princeton.edu)

R.G., 0000-0002-8635-8294; E.N.K., 0000-0002-8156-6959; K.V.Y., 0000-0002-0718-0775; L.V.O., 0000-0002-7422-4387; A.A.K., 0000-0002-5866-3574; J.B., 0000-0002-9278-5532; M.Z., 0000-0002-4996-4500; P.S., 0000-0001-5704-2349; Y.V.S., 0000-0002-3643-9889

Handling Editor: Cassandra Extavour
Received 23 November 2020; Accepted 22 July 2021

Development (2021) 148, dev198788. doi:10.1242/dev.198788

cells in the cyst so that all nuclei are clustered towards its basal side (relative to the apical-basal polarity of the testes). Basal bodies, which function as microtubule nucleation centers, are located on the apical side of the nuclei. They initiate the assembly of the flagellar axonemes that grow towards the apical tip of the testes. The axonemes elongate until they almost reach this tip and then normally cease to grow (Fabian and Brill, 2012; Tokuyasu, 1974, 1975; Tokuyasu et al., 1972). During the elongation phase, *orb2* transcript and protein are concentrated in a ring near the tip of the growing axoneme. Similar to other gene products that are localized during axoneme growth, *orb2* transcript and protein form a 'comet tail' extending back through the axonemes towards the nuclei clustered at the basal pole of the spermatids (Barreau et al., 2008; Xu et al., 2012). Once elongation is complete, the process of individualization begins. Individualization is accomplished by the assembly of a special structure called the individualization complex (IC). The IC consists of 64 actin cones that assemble around the nuclei at the basal cap of spermatids. The IC then travels down the bundled flagellar axonemes, ensheathing each in a plasma membrane and pushing the excess cytoplasm into a waste bag. During this phase, the spermatid nuclei undergo a series of morphological transitions that alter the protein composition of their chromatin (Fabian and Brill, 2012; Fabrizio et al., 1998; O'Donnell, 2014; Rathke et al., 2007).

Analysis of *orb2* mutants indicates that this gene has important functions at several steps of spermatogenesis (Xu et al., 2012, 2014). The *orb2* null mutants show no obvious defects in spermatocytes during the prolonged G2 leading up to meiosis I, but these cells are arrested early in meiosis I, accumulating high levels of nuclear Cyclin A. In addition to being required in meiosis, Orb2 has also been implicated in spermatid differentiation. It has a role in the initial polarization of cells in the 64-cell cyst, and at this step it is thought to have two different functions. One is in orienting cyst polarization relative to the apical-basal axis of the testis. The other is in the polarization of germ cells in the cyst so that their nuclei cluster together at one side of the cyst, while microtubule nucleation centers (basal bodies) are oriented so that microtubule assembly is directed towards the other (apical) side of the cyst. Once the 64-cell cyst is properly polarized, *orb2* contributes to the elongation of the flagellar axonemes. It is required for localizing transcripts in a comet pattern in the growing flagellar axonemes and activating their translation. The transcripts for which localization and translation depend on Orb2 include *orb* and *aPKC* mRNAs (Xu et al., 2012, 2014). *orb2* mutants have defects in termination of flagellar axoneme growth and in the assembly of the ICs.

Studies on the other fly CPEB protein, Orb, have shown that it has a positive autoregulatory activity: Orb binds to sequences in the 3′UTR of its own transcript, localizes the transcript to the developing oocyte, and controls its on-site translation. This 3′UTR-dependent autoregulatory activity helps drive oocyte specification in the newly formed 16-cell cysts, and at later stages of oogenesis it is important for ensuring that sufficient levels of Orb protein are localized to the developing oocyte (Barr et al., 2019; Tan et al., 2001). Similar to the *orb* 3′UTR, most of the *orb2* 3′UTRs are long and carry multiple CPE-like elements. Moreover, we and other authors have found that Orb2 is associated with *orb2* transcript *in vivo* (Mastushita-Sakai et al., 2010; Stepien et al., 2016; Xu et al., 2012). These observations raise the question of whether the *orb2* 3′UTR is important for the functioning of *orb2* during spermatogenesis. To address this question, we used the CRISPR/Cas9 system to delete the *orb2* 3′UTR and analyzed the mutants for the effect of this deletion on spermatogenesis.

RESULTS

Deletion of the *orb2* 3′UTR

The *orb2* gene is predicted to encode five transcript species that differ in their transcription start sites, splicing patterns and the lengths of their 3′UTRs. Only one of them, *orb2*-RA, encodes the smaller 60-kDa Orb2A isoform. As shown in Fig. 1, *orb2*-RA has a very short 3′UTR that lacks not only the canonical UUUUAU CPE, but also other known CPE-like motifs. All other *orb2* transcripts encode the larger 75-kDa Orb2B isoform. One of them, *orb2*-RB, has a short 580-nt 3′UTR that lacks the canonical UUUUAU CPE, but contains two CPE-like motifs, UUUUUGT and UUUUUGUU, that are reported to be enriched in Orb2-associated mRNAs (Stepien et al., 2016). The *orb2*-RC transcript has a 1563-nt 3′UTR, whereas the two remaining transcripts, *orb2*-RD and *orb2*-RH, have 3′UTRs of 3826 and 5791 nt, respectively. The distribution of canonical CPEs in these transcripts is different. There are one canonical and six non-canonical CPEs in the 1563-nt RC 3′UTR, whereas the two larger 3′UTRs have 27 and 37 CPE-like sequences, respectively, including nine canonical UUUUAU motifs.

We designed a deletion that selectively removes the bulk of the 3′UTR sequence. As shown in Fig. 1, the CRISPR/Cas9 deletion excises a 4522-bp DNA segment that includes all canonical CPEs in *orb2*-RC, *orb2*-RD and *orb2*-RH. As the proximal endpoint of the

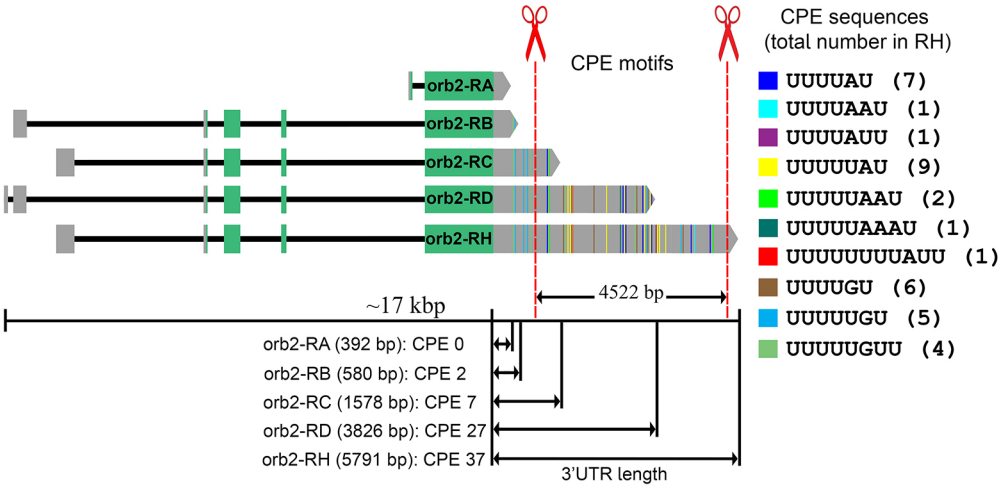

Fig. 1. Structure of *orb2* transcripts and location of the 3′UTR deletion. The *orb2* gene encodes five distinct mRNA species that differ in the length of their 3′UTRs and contain different sets of canonical and non-canonical CPE sequences (indicated on the right). Cutting sites for CRISPR/Cas9 gene modification are indicated. CPE motifs were taken from the CPEB CLIP dataset (Stepien et al., 2016).

Development (2021) 148, dev198788. doi:10.1242/dev.198788

deletion is well downstream of the *orb2*-RA and *orb2*-RB polyadenylation signal, these transcripts should not be affected. *orb2*-RC, *orb2*-RD and *orb2*-RH are expected to acquire a common polyA signal and the 3′UTR sequence upstream of the deletion breakpoint, which is 1008 nt long and contains five non-canonical but Orb2-enriched CPEs (UUUUUGT or UUUUUGUU).

In the initial fly stock, the deleted DNA was replaced by the *DsRed* gene flanked by loxP sites and an attP sequence, and *DsRed* was then excised. The deletion was verified by sequencing, and the resulting mutation was designated $orb2^R$. Five independent CRISPR/Cas9-mediated deletions were recovered. All five lines showed similar phenotypes, including a significant decrease in male fertility, scattered nuclei at late stages of spermatogenesis, and partially filled seminal vesicles. One of the lines was selected for further study.

Most $orb2^R$ males are sterile

Whereas *orb2* null alleles are semi-lethal, with only a few flies surviving to adulthood, the $orb2^R$ mutation does not appear to affect any essential processes during development, as the number of homozygous $orb2^R$ flies reaching the adult stage is close to that in wild-type (WT) flies (Fig. S1). However, the overall fertility in the $orb2^R$ males was found to be reduced (approximately 10% of males were fertile) (Fig. S2). Measurement of the fertility of individual $orb2^R$ males revealed that ∼75% are completely sterile (Fig. 2A). Although the remaining males were fertile, the number of progeny they produced was significantly lower than WT. WT males typically have an average of 72 offspring, whereas the few $orb2^R$ males that were fertile had on average only ∼20 offspring (Fig. 2B).

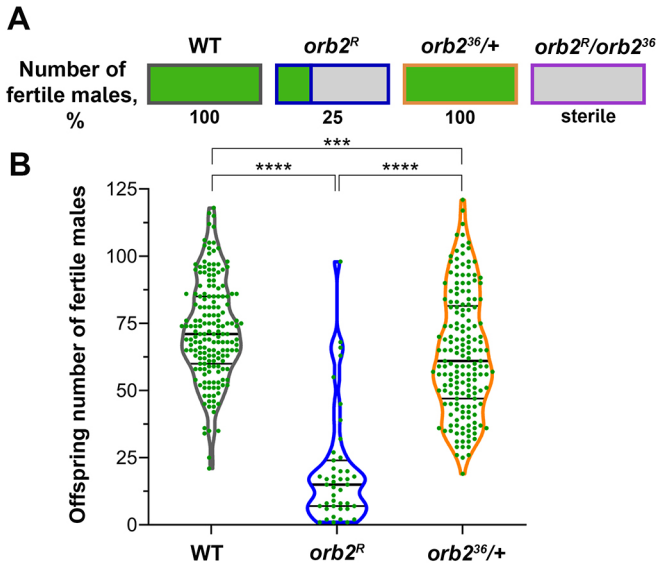

Fig. 2. Fertility assay. (A) Male fertility assay. Individual WT, $orb2^R$, $orb2^{36}$/+ and $orb2^R/orb2^{36}$ males were mated with two WT virgin female flies. The number of males that had any progeny was counted (WT, *n*=287; $orb2^R$, *n*=358; $orb2^{36}$/+, *n*=175; $orb2^R/orb2^{36}$, *n*=145). All data are presented as percentages of the total number of males tested. (B) Assay for the number of progeny from individually mated males. Individual males of the WT, $orb2^R$ and $orb2^{36}$/+ genotypes were crossed to WT virgin female flies and the number of progeny from each individual male was estimated (to score the number of $orb2^R$ offspring, only fertile males were taken into account). The number of tested WT males was 175; $orb2^{36}$/+ males, 173; fertile $orb2^R$ males, 43. The horizontal lines show three quartiles Q1-Q3. Statistical analysis was performed using an unpaired two-tailed *t*-test; ***P<0.001, ****P<0.0001.

We also tested the fertility of male flies that are *trans*–heterozygous for $orb2^R$ and a deletion, $orb2^{36}$, that removes the *orb2* gene. This semi-vital allele determines complete male sterility (Xu et al., 2012). As would be expected if the $orb2^R$ mutation is responsible for the reduced fertility in homozygous males, complementation with $orb2^{36}$ was not observed. Instead, the phenotype became stronger, and the *trans*-heterozygous males were completely sterile (Fig. 2A).

The accumulation of *orb2* transcript and protein is reduced in $orb2^R$ testes

To understand better the nature of the spermatogenesis defects in $orb2^R$, we examined the expression of *orb2* mRNA and protein. We used RT-qPCR to measure the levels of *orb2* mRNA in WT and $orb2^R$ testes relative to a reference transcript, *Gapdh2* mRNA, which lacks canonical CPEs. Fig. 3A shows that the level of *orb2* mRNA in $orb2^R$ testes was reduced to approximately half that in WT. This is likely due to decreased stability of the mRNA, as the level of *orb2* primary transcripts (detected with primers located at the last intron-exon junction) in $orb2^R$ testes was close to that in WT. Because the $orb2^R$ mutation alters the structure and polyadenylation of mRNAs encoding the 75-kDa Orb2 protein, we examined the expression of this isoform in testis lysates (Fig. 3B). Quantitative analysis (Fig. 3C) showed that the level of the 75-kDa Orb2 isoform in mutant testes was approximately half that of WT, similar to $orb2^R$ mRNA.

The experiments described above indicate that deletion of *orb2* 3′UTR sequences results in a reduction in both mRNA and protein levels. This finding raises the possibility that most $orb2^R$ males are sterile because there are insufficient amounts of *orb2* gene products. However, as shown in Fig. 2, there is no evidence of a strong haploinsufficiency as males heterozygous for the *orb2* deletion ($orb2^{36}$) are completely fertile and produce almost as many offspring as WT males. To confirm that $orb2^{36}$/+ testes have the expected reduction in *orb2* gene products, we compared *orb2* mRNA and protein levels in WT and $orb2^{36}$/+. As shown in Fig. 3A, the amount of *orb2* mRNA in $orb2^{36}$/+ testes was only ∼25% of that in WT. Similar results were obtained when we compared protein levels in WT and either $orb2^{36}$/+ or $orb2^R/orb2^{36}$. The level of Orb2 protein in $orb2^{36}$/+ was about one-third of that in WT.

These findings show that the reductions in *orb2* mRNA and protein in $orb2^{36}$/+ males are greater than that observed in $orb2^R$ homozygotes, even though all $orb2^{36}$/+ males are fertile. Thus, the fact that the levels of *orb2* gene products are lower than WT in $orb2^R$ testes cannot in itself be responsible for the sterility of most $orb2^R$ males.

The *orb2* 3′UTR is required for proper *orb2* transcript and protein localization during spermatid differentiation

To understand why most $orb2^R$ males are sterile, we examined *orb2* mRNA and protein localization during spermatogenesis. The pattern of their accumulation in premeiotic and meiotic cysts was found to be similar to that in WT, with $orb2^R$ mRNA and protein expression being upregulated in 16-cell spermatocyte cysts and the protein being more or less evenly distributed throughout the cytoplasm. However, the amounts of mRNA and protein in the pre-meiotic and meiotic $orb2^R$ cysts (scheme in Fig. 4A) appeared to be reduced, compared with WT (Fig. 4B,C).

Despite this reduction, $orb2^R$ differs from the null allele $orb2^{36}$, in that spermatogenesis is not arrested prior to meiosis I; instead, both meiotic divisions appear to be normal, and 64-cell cysts are formed. To confirm this observation, we examined the pattern of Cyclin A

Development (2021) 148, dev198788. doi:10.1242/dev.198788

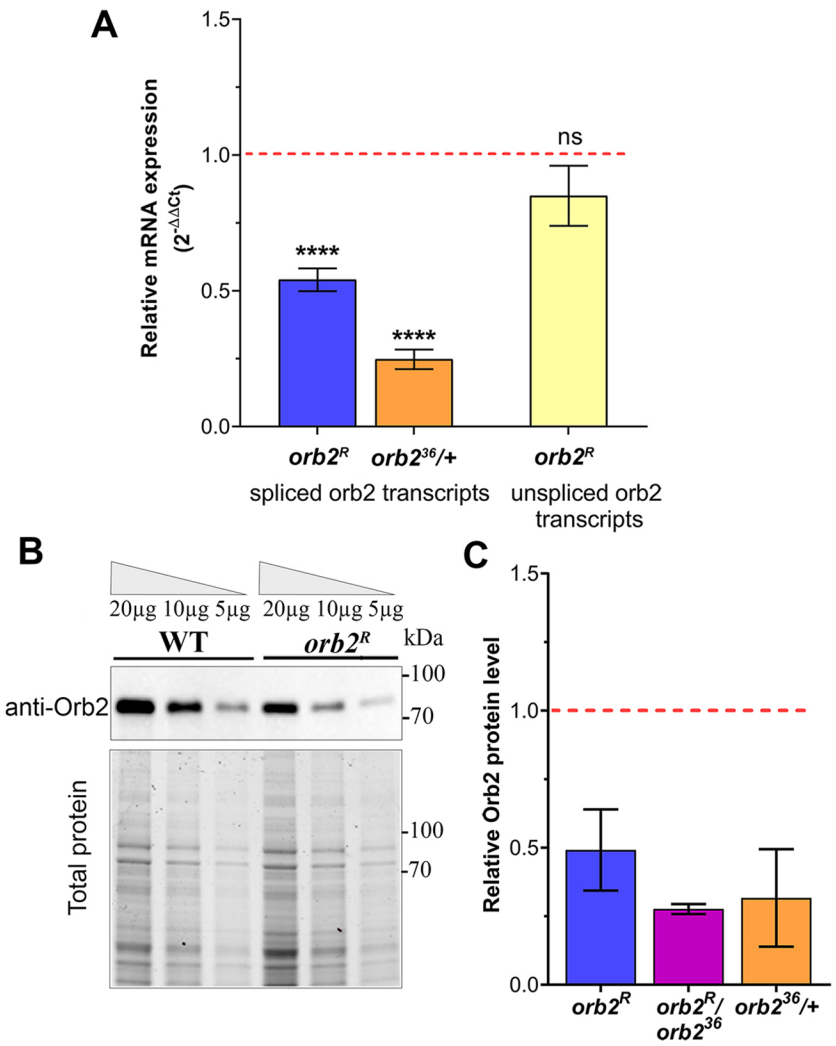

Fig. 3. Deletion in the 3′UTR of *orb2* reduces its expression in testes. (A) The level of total *orb2* mRNA in *orb2*^{R} and *orb2*^{36}/+ mutant testes and the level of primary *orb2* transcripts in *orb2*^{R} mutant testes. Data were first normalized to the expression of *Gapdh2* in testes and expressed as the mean fold change ($2^{-\Delta\Delta Ct}$) in mutant testes relative to control ones (red dashed line) (spliced isoform: WT, *n*=29; *orb2*^{R}, *n*=27; *orb2*^{36}/+, *n*=18; unspliced isoform: WT, *n*=10; *orb2*^{R}, *n*=10). The error bars represent s.e.m. Unpaired two-tailed *t*-test: ****P<0.0001; ns, P>0.05. (B) Western blot analysis of Orb2 protein in a dilution series of testes lysates (total protein level is indicated above). Part of a gel stained for total protein is shown below. (C) Densitometry analysis of Orb2 level normalized to total protein level in mutant testes compared with WT testes (red dashed line). Quantitative data of western blotting were obtained from independent biological replicates (*orb2*^{R}, *n*=7; *orb2*^{R}/*orb2*^{36}, *n*=4) and expressed as mean±s.d.

and B accumulation. As found in our previous study, the 16-cell cysts in *orb2*^{36} testes had an abnormal nuclear localization of Cyclin A and B (Xu et al., 2012). In contrast, these proteins in *orb2*^{R} were localized in the cytoplasm, as in WT (Fig. 4D,E).

Although spermatogenesis appears to be unaffected through the completion of meiosis, a series of abnormalities became evident once the spermatids began to differentiate. One of these abnormalities was in the elongation of the spermatid tail.

After meiosis is complete, the flagellar axonemes of spermatid cysts begin to elongate towards the apical end of the testis in WT (scheme in Fig. 4A). During this period of spermatid development, *orb2* mRNAs and proteins become concentrated in a band near the tip of the growing flagellar axonemes, with a comet tail extending back towards the nuclei (Fig. 5A-D). A different result was obtained in *orb2*^{R} mutant testes or when *orb2*^{R} was in *trans* to the *orb2*^{36} deletion. Instead of concentrating in a band near the tip of the elongating flagellar axonemes, *orb2*^{R} transcripts were distributed with opposite polarity and seen in higher amounts closer to the basal end of the tail. Likewise, Orb2 protein in WT was concentrated in a band near the tip, but this was not observed in *orb2*^{R} or in *orb2*^{R}/*orb2*^{36}. In fact, the levels of the protein were lower near the apical tip than in more basal regions of the spermatid tail. These findings indicate that the deleted 3′UTR sequences are important for the proper localization of *orb2* mRNAs and proteins during the process of spermatid tail elongation.

In addition to these defects in *orb2* mRNA and protein localization, it is also worth noting that the morphology of the elongated spermatid tails in *orb2*^{R} and *orb2*^{R}/*orb2*^{36} was often different from WT (Fig. 5C-E). In WT, the thickness (diameter) of the tail in the region closest to the apical tip was similar to that in more basal portions of the tail. This likely reflects the uniform elongation of the different flagellar axonemes in the growing spermatid tail. In *orb2*^{R} and *orb2*^{R}/*orb2*^{36}, in contrast, the spermatid tails often appeared to be tapered into a point at the tip, as if the extent of elongation of individual flagellar axonemes in the spermatid tail was uneven. If this inference is correct, it suggests that *orb2* is required for coordinating flagellar axoneme extension in the growing spermatid tails. This may explain why both *orb2* mRNA and protein concentrate in a band near the tip of the elongating tail in WT.

The *orb2*^{R} mutation affects the spermatid localization of other transcripts and proteins

A number of other transcripts and proteins have been found to have a comet-like distribution in elongating spermatid tails (Barreau et al., 2008; Xu et al., 2012). One of these is *orb*, which encodes the other fly CPEB protein. Consistent with a role in regulation of *orb* mRNA localization and/or translation, *orb* mRNAs can be immunoprecipitated with Orb2 antibodies from WT testis extracts (Xu et al., 2012). In WT, *orb* mRNAs preferentially accumulated in a

Development (2021) 148, dev198788. doi:10.1242/dev.198788

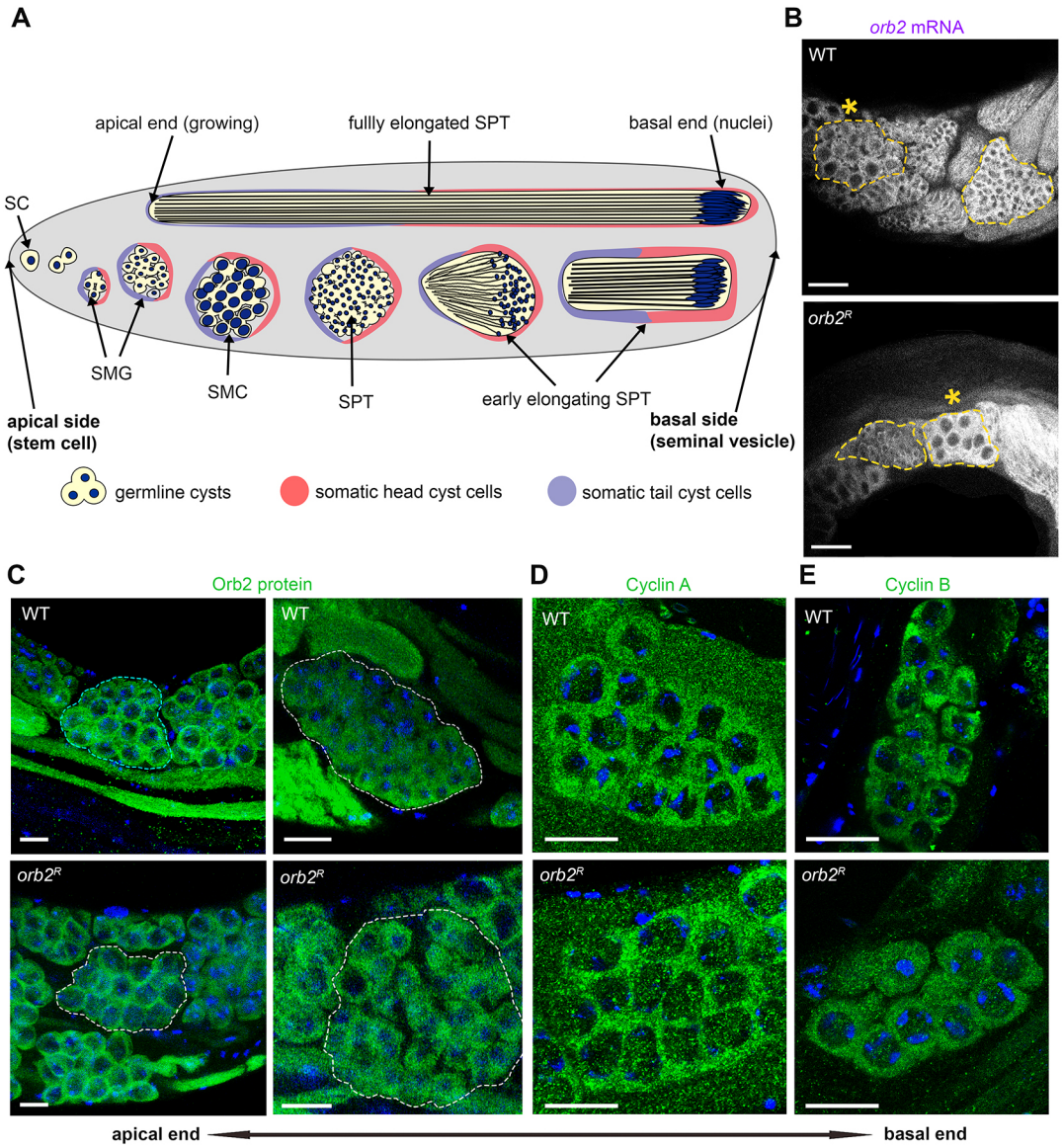

Fig. 4. Orb2 protein and *orb2* mRNA in premeiotic and meiotic cysts. (A) Scheme of spermatogenesis. SC, stem cell; SMC, spermatocyte; SMG, spermatogonium; SPT, spermatid. (B) FISH for *orb2* mRNA localization in primary spermatocytes (16-cell premeiotic cysts) within the area indicated by an asterisk and in secondary spermatocytes (32-cell meiotic cyst) within the highlighted area (without an asterisk) in WT and $orb2^R$ testes. Except for a slight decrease in the signal, the mutants show no obvious changes in the localization of *orb2* mRNA at these stages (WT, *n*=25; $orb2^R$, *n*=18). (C) Whole-mount staining of testes with Orb2 antibodies shows that the level of Orb2 protein in primary spermatocytes (left) in $orb2^R$ is reduced, compared with WT, with the pattern of its localization remaining unchanged; the same is also true of secondary spermatocytes (right) (WT, *n*=20; $orb2^R$, *n*=21). Dashed lines delineate premeiotic and meiotic cysts. (D) Staining with antibodies against Cyclin A protein. Cyclin A is predominantly localized in the cytoplasm of 16-cell cysts both in WT and $orb2^R$ flies (WT, *n*=15; $orb2^R$, *n*=17). (E) Staining with antibodies against Cyclin B protein. Both WT and $orb2^R$ flies show cytoplasmic localization of Cyclin B in cysts (WT, *n*=14; $orb2^R$, *n*=13). Scale bars: 40 µm (B); 30 µm (C); 50 µm (D,E).

band near the tip of the elongating flagellar axonemes (Fig. 6A,A′). Abnormalities in the localization of *orb* transcript and the expression of Orb protein were evident in $orb2^R$ testes. Instead of being localized to the tip of the elongating spermatid tails, *orb* mRNAs in $orb2^R$ were distributed over a major part of the tail (Fig. 6A,A′). In line with the disruption in transcript localization, Orb proteins did not show preferential accumulation at the tip of the flagellar axonemes and appeared prematurely. As shown in Fig. 6B, the tips of the flagellar axonemes in $orb2^R$ testes (indicated by brackets) contained little Orb protein. Instead, Orb either accumulated in an intermediate position or was distributed over much of the flagellar axonemes. Even more extreme disruptions in the localization of *orb* mRNA and Orb protein were evident in testes of $orb2^R/orb2^{36}$ males (Fig. 6A,B).

The fly homolog of the mammalian DAZ fertility factor is the RNA-binding protein Boule (Bol) (Cheng et al., 1998). The Bol protein can be co-immunoprecipitated with Orb2 in an RNase-resistant complex, and during the spermatid elongation phase it colocalizes with Orb2 in a region near the tip of the growing flagellar axonemes (Xu et al., 2012). We also observed a comet-like gradient that extends back from the tip towards the nuclei on the basal side of spermatids (Fig. 6C). This pattern of localization was not observed in $orb2^R$ testes. Unlike in WT, Bol was not preferentially localized close to the end of elongating axoneme (Fig. 6C, brackets). Instead, it was distributed more or less uniformly over a major part of the spermatid tail. As was observed for Orb, Bol was also not properly localized in $orb2^R/orb2^{36}$ testes.

Development (2021) 148, dev198788. doi:10.1242/dev.198788

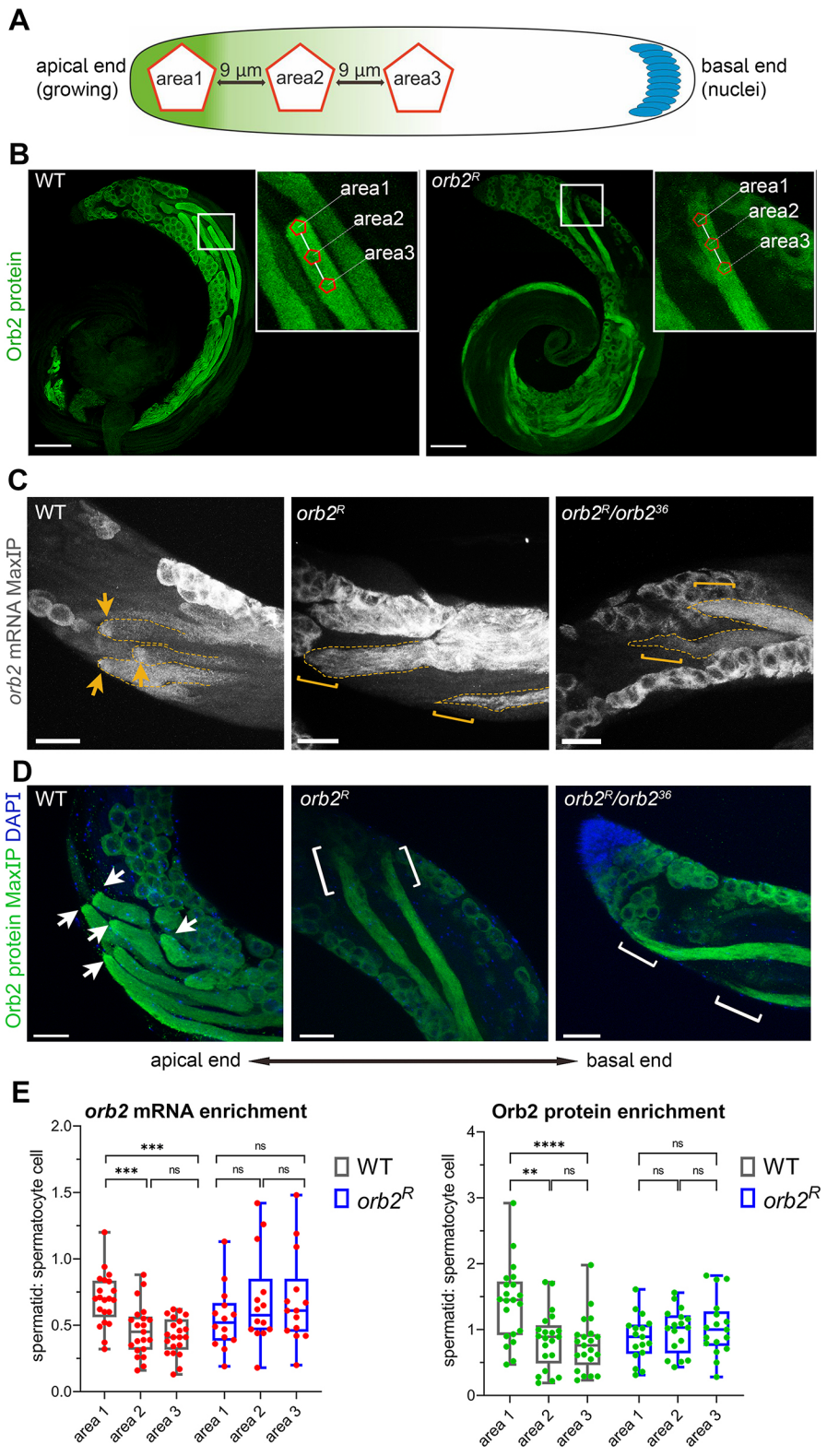

Fig. 5. The *orb2* 3′UTR is required for localization of mRNA and protein in spermatid cysts. (A) The areas of *orb2* mRNA and protein localization analyzed within a spermatid cyst. (B) Maximum intensity projections of the Orb2 protein and enlarged images (insets) of the regions under study at the end of spermatid tails marked in red. (C,D) Maximum intensity projections of *orb2* mRNA (C) and Orb2 protein (D) within spermatid cysts in WT, $orb2^{R}$ and $orb2^{R}/orb2^{36}$ testes. Dashed lines delineate spermatid cyst tail ends. Arrows indicate mRNA or protein accumulated at the ends of WT spermatid cysts; brackets indicate spermatid cyst tail ends without corresponding mRNA or protein accumulation in mutant testes. (E) Quantification of *orb2* mRNA and protein distribution along the spermatid cyst. Box plots of *orb2* mRNA and protein levels in the different areas of spermatid cysts relative to those in spermatocytes for WT (n=21) and $orb2^{R}$ (n=14). Unlike WT, $orb2^{R}$ spermatid cysts showed a decreased level of *orb2* mRNA and protein in analyzed area 1, compared with areas 2 and 3, and no longer demonstrated the gradient comet-like pattern of localization. The box plot shows the median (line within the box), the interquartile range (the box), and the 10th and the 90th percentiles (whiskers). ****P<0.0001, ***P<0.0005, **P<0.005; ns, not significant. Scale bars: 100 µm (B); 40 µm (C,D).

Early steps in spermatid cyst polarization are disrupted in $orb2^{R}$

The defects in localization of mRNAs and proteins in the elongating spermatid tails as well as the abnormal morphology of the tails prompted us to examine early steps in the polarization of the 64-cell spermatid cysts. Even before spermatid tails begin to elongate, the 64-cell cysts must become polarized, and this is one of the initial steps in spermatid differentiation. When they were first formed, the 64-cell cysts in $orb2^{R}$ resembled those in WT. The haploid cells in WT and $orb2^{R}$ cysts had a round shape and were ∼10 µm in diameter. Subsequently, the cyst begins to polarize. In WT, all of the nuclei cluster towards the basal side of the cyst, whereas the basal body associated with each nucleus localizes to the apical side of the cysts and initiates the assembly of the flagellar axoneme.

Development (2021) 148, dev198788. doi:10.1242/dev.198788

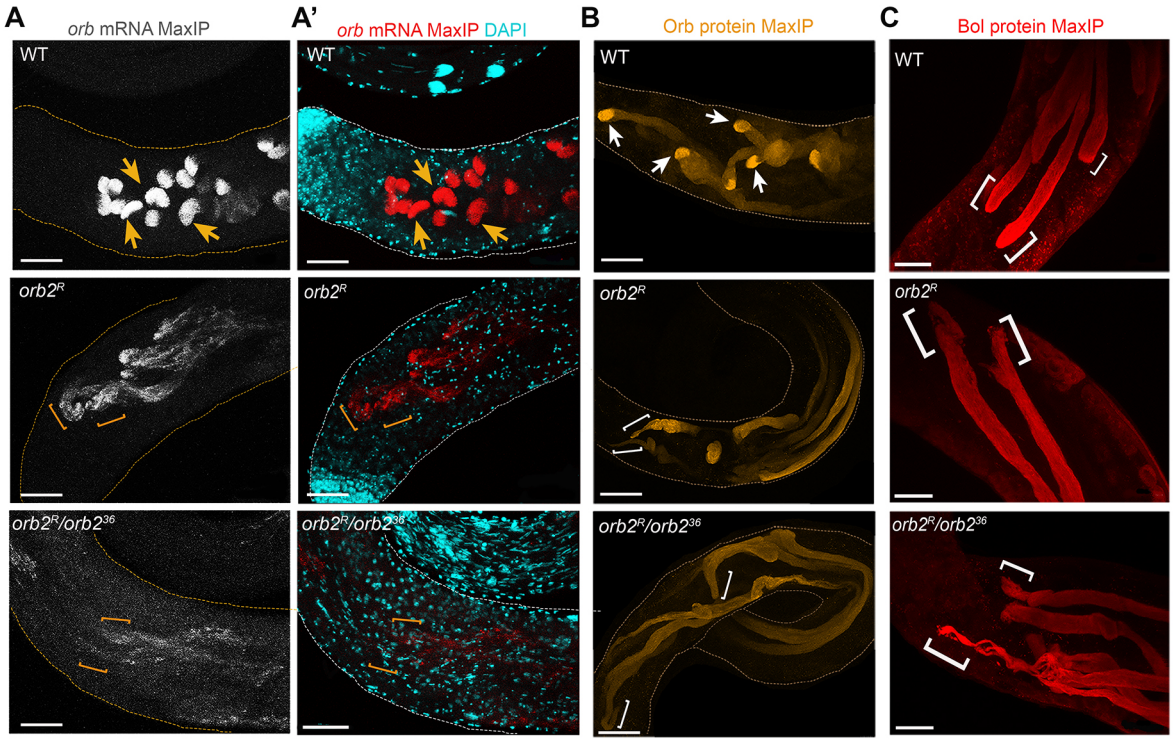

Fig. 6. Localization of other transcripts and proteins in testes depends on *orb2* 3′UTR. (A,A′) Maximum intensity projections of *orb* mRNA in WT (*n*=15), *orb2*^{R} (*n*=24) and *orb2*^{R}/*orb2*^{36} (*n*=20) testes. A high fluorescence signal is observed at the ends of WT spermatid tails (arrows), whereas this pattern in mutant testes is lost (brackets indicate the end of mutant spermatid tails), and *orb* mRNA is distributed uniformly. (B) Maximum intensity projections of Orb protein in WT (*n*=30), *orb2*^{R} (*n*=28) and *orb2*^{R}/*orb2*^{36} (*n*=13) testes. Arrows indicate Orb protein localization at the ends of WT spermatid cysts; brackets indicate the spermatid cyst tail ends without Orb protein accumulation in mutant testes. (C) Maximum intensity projections of Boule protein in WT and mutant testes. Boule is enriched at the ends of elongated spermatid cysts in WT (*n*=9) but is uniformly distributed along spermatid cysts in *orb2*^{R} (*n*=22) and *orb2*^{R}/*orb2*^{36} (*n*=32). Brackets indicate the ends of spermatid cyst tails. Scale bars: 50 µm (A,A′,B); 40 µm (C).

The flagellar axonemes then begin elongating towards the apical end of the testis and ultimately form elongated cells that are almost 2 mm long (Fabian and Brill, 2012; Tokuyasu, 1975; Tokuyasu et al., 1972).

We used antibodies against βNACtes proteins to examine the polarization and cytoskeletal organization of 64-cell cysts that have just begun the process of differentiation. Several closely related βNACtes proteins are expressed at high levels in testes and are thought to function as part of a ribosome-associated protein-folding chaperone (Kogan et al., 2017). As illustrated for WT in Fig. 7, βNACtes proteins preferentially assemble into a series of distinct and evenly spaced longitudinal stripes along the apical-basal axis of the polarizing spermatid cyst. Presumably, this regular organization reflects some kind of association with the nascent flagellar axonemes or with some other repeating cytoskeletal structures in the cyst. This stripe pattern was not as evident at the basal end of WT cysts where the arrangement of the βNACtes proteins appeared less organized, probably because the proteins are intermingled with basal cluster of spermatid nuclei.

These stereotypic features of newly polarized cysts were disrupted in *orb2*^{R} and *orb2*^{R}/*orb2*^{36}. Instead of clustering at the basal tip of the polarizing cysts, the nuclei were found scattered along the apical-basal axis in a subset of the *orb2*^{R} cysts, with such scattering being observed in all *orb2*^{R}/*orb2*^{36} cysts. The regularly spaced stripes of βNACtes proteins in the nascent spermatid tails on the apical side of the cyst were also disrupted. Whereas the βNACtes proteins are assembled into a series of longitudinal stripes in WT, these stripes were either absent or interrupted in many of the *orb2*^{R} cysts. The extent of disruptions in the organization of βNACtes proteins was even greater in *orb2*^{R}/*orb2*^{36} cysts (Fig. 7). These findings indicate that proper cyst polarization requires the *orb2* 3′UTR and raise the possibility that some of the subsequent defects in spermatid tail elongation result, at least in part, from this initial failure in polarization.

Late steps in nuclear maturation are abnormal in *orb2*^{R}

As the spermatid tails grow, the nuclei in WT undergo a series of morphological changes. Initially they have a spherical shape but then transition through several intermediate stages, including the leaf, early canoe, late canoe and, finally, needle stage (Fabian and Brill, 2012; Tokuyasu, 1975; Tokuyasu et al., 1972). Along with these morphological changes, the nuclei coalesce into a tight bundle to form an inverted cap-like structure (Fig. 8A) (Tokuyasu et al., 1972). In *orb2*^{R} testes, most of the nuclei in the cysts appeared to progress to the needle stage, but their subsequent coalescence into the cap-like structure was defective, with only a few exceptions (~10% of the testes) (Fig. 8A,B). In ~45% of the testes, only a subset of the spermatid cysts had nuclei that coalesced into a cap-like structure; in other cysts, the nuclei were scattered or displayed only partial coalescence. No coalesced nuclei were found in the remaining testes (~45%). When *orb2*^{R} was *trans* to *orb2*^{36}, scattered nuclei were observed in all of the cysts (Fig. 8B).

ICs are not properly assembled in *orb2*^{R} mutants

When flagellar axoneme elongation is complete, the spermatids enter the individualization stage. The actin-rich IC is assembled around each nucleus in a cap-like structure. The IC then begins to

Development (2021) 148, dev198788. doi:10.1242/dev.198788

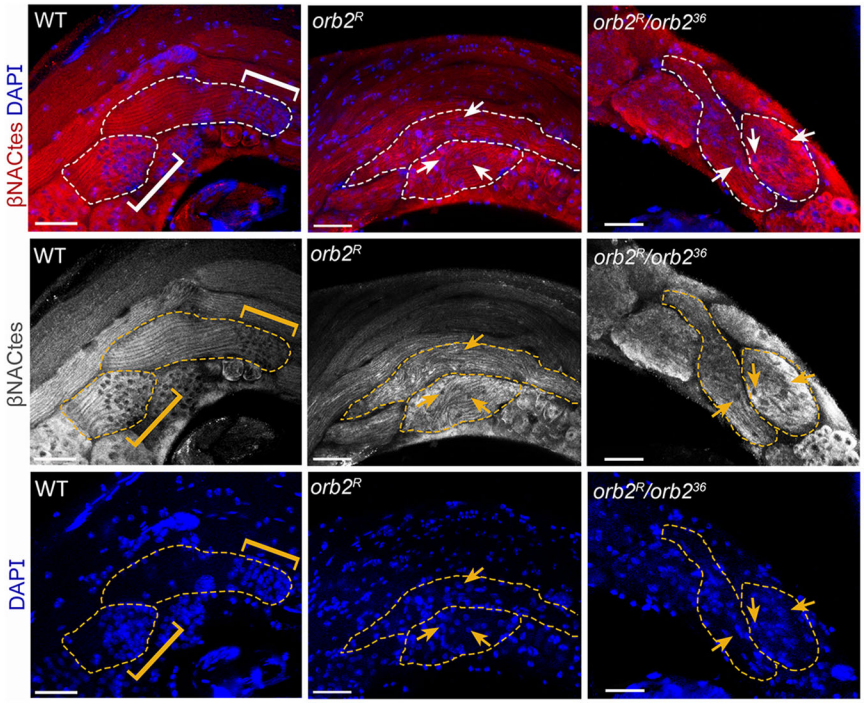

Fig. 7. The *orb2* 3′UTR is required for nuclear polarization in early elongated spermatids. Whole-mount testis staining with βNACtes antibodies, which mark germline cells in testes (Kogan et al., 2017). Chromatin was stained with DAPI. Brackets indicate the areas of nuclear polarization at the basal ends of early elongated spermatid cysts in WT (*n*=29). In contrast, the distribution of nuclei (arrows) along elongated spermatid is uniform in $orb2^{R}$ (*n*=34) and $orb2^{R}/orb2^{36}$ (*n*=36). Note also changes in the longitudinal βNACtes protein stripes in the mutants. Dashed lines delineate early elongated spermatid cysts. Scale bars: 30 µm.

move down the flagellar axonemes, investing each spermatid with its own plasma membrane and extruding the excess cytoplasm into a 'waste bag' (Fabrizio et al., 1998; Noguchi and Miller, 2003). ICs were successfully assembled in only about 15% of the $orb2^{R}$ testes (Fig. 8C,D). In the remaining $orb2^{R}$ testes, either only a subset of the elongated spermatids assembled an IC or there was no IC assembly at all. As indicated in Fig. 8C, IC assembly was completely disrupted in $orb2^{R}/orb2^{36}$ *trans*-heterozygotes testes.

Consistent with the defects in the assembly of ICs, only ∼30% of seminal vesicles in $orb2^{R}$ were filled with mature sperm; others were either empty or filled only partially (Fig. 8E,F). Seminal vesicles in $orb2^{R}/orb2^{36}$ contained no sperm. These findings are consistent with data on the fertility of $orb2^{R}$ and $orb2^{R}/orb2^{36}$ males.

$orb2^{R}$ shifts expression of *yuri*, required for early spermatid polarization

To gain further insights into the post-meiotic defects of spermatogenesis in $orb2^{R}$, we assessed expression of the five genes – *yuri*, *unc*, *soti*, *Bruce* and *orb* – that function at different stages of spermatid differentiation. Similar to *orb2*, the *unc* and *yuri* genes are required for spermatid polarization, which is one of the first steps in spermatid differentiation (Baker et al., 2004; Barreau et al., 2008), and *yuri* has been implicated in orientation of spermatid elongation within the testis. Misoriented actin cones form during individualization in the *yuri* (Texada et al., 2008), $orb2^{36}$ (Xu et al., 2014) and $orb2^{R}$ (Fig. 8C) mutants. The genes *soti* and *Bruce* function at a later step, after spermatid elongation is complete, and are required for proper functioning of the IC (Kaplan et al., 2010). As shown in Fig. 9, the levels of *yuri* mRNAs were elevated in $orb2^{R}$, and *unc* mRNA levels also appeared to be increased, at least marginally. In contrast, changes in the levels of *soti* and *Bruce* mRNAs were minimal, as was also the case with *orb* mRNA. These findings raise the possibility that some of the abnormalities in spermatid differentiation in the $orb2^{R}$ mutant may arise from changes in the relative balance of mRNAs encoding factors required for this process.

DISCUSSION

The localization of gene products to the cellular domains where their functions are required is crucial for the establishment of cell polarity. Depending on the context, a variety of mechanisms can be employed to ensure proper targeting (McCaffrey and Macara, 2009; Nelson, 2003). One of them involves the on-site translation of localized transcripts. After their synthesis and export from nuclei, the translationally silenced transcripts are localized either by an active microtubule-dependent mechanism or by passive diffusion. Once the transcripts are on site, RNA-binding proteins interact with them to regulate their translation. The CPEB protein family is a group of translation factors that help anchor and control the on-site translation of localized transcripts (Barr et al., 2016; Besse and Ephrussi, 2008; Lantz et al., 1992; Lasko, 2012; Martin and Ephrussi, 2009; St Johnston, 2005). CPEBs recognize CPE elements in the 3′UTR of localized transcripts and can function to repress or activate their translation, depending on the context. The canonical CPE sequence is UUUUAU; however, several variants of this motif are enriched in transcripts that are found associated with different members of the CPEB family. *Drosophila* has two CPEB proteins, Orb and Orb2. The former has essential functions during oogenesis and is required for the translation of multiple oocyte-localized transcripts (Chang et al., 1999, 2001; Christerson and McKearin, 1994). Moreover, it also has autoregulatory activity, with Orb binding to the *orb* transcript 3′UTR and activating its own expression (Tan et al., 2001). This autoregulatory activity plays a key role in oocyte specification, and *orb* mutants that lack portions of the *orb* transcript 3′UTR fail to specify an oocyte (Barr et al., 2019).

Unlike *orb*, *orb2* has no essential function in oogenesis; however, it is required at several stages of spermatogenesis (Xu et al., 2012, 2014). Here, we have investigated the role of *orb2* 3′UTR sequences in the transcripts encoding the larger 75-kDs isoform in *orb2* activity during spermatogenesis. Four transcripts (*orb2*-RB, *orb2*-RC, *orb2*-RD and *orb2*-RH) are predicted to encode the 75-kDa isoform. They carry 3′UTRs of different lengths with different numbers of CPE and CPE-like elements, from two (*orb2*-RB) to

Development (2021) 148, dev198788. doi:10.1242/dev.198788

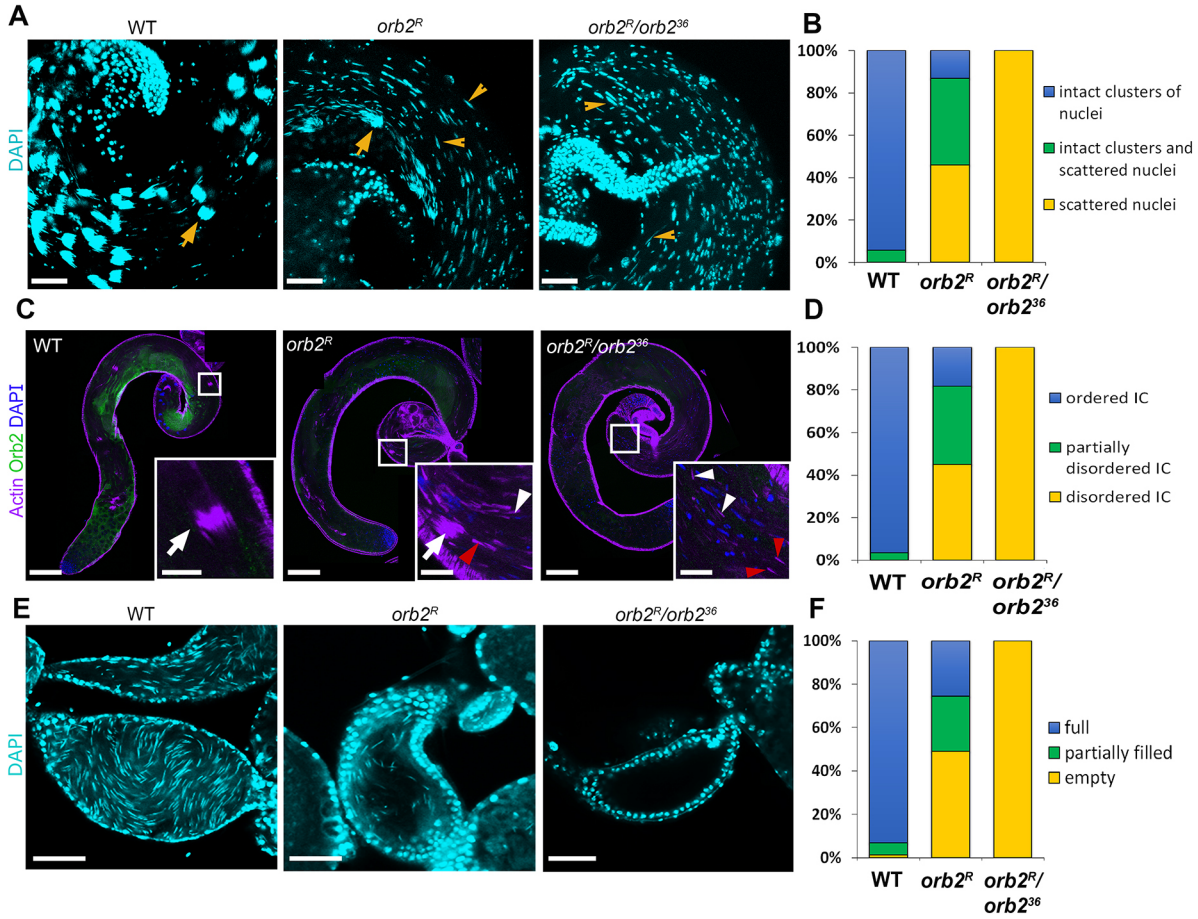

Fig. 8. Compaction of nuclei, formation of the IC, and seminal vesicle filling are disrupted in *orb2*^{R} testes. (A) Confocal slices of immunostained whole-mount testis preparations. Chromatin was stained with DAPI. Arrows indicate a condensed spermatid nuclear bundle in WT and partially assembled spermatid nuclear bundles in *orb2*^{R}. Arrowheads indicate scattered nuclei incapable of compaction in mutant spermatids. (B) The frequency of spermatids defective in nuclei clustering in WT (*n*=86), *orb2*^{R} (*n*=61) and *orb2*^{R}/*orb2*^{36} (*n*=57). (C) ICs are not properly assembled in *orb2*^{R} and *orb2*^{R}/*orb2*^{36}. Confocal slices of whole-mount testis preparations are shown. Chromatin was stained with DAPI (blue); actin cones were stained using phalloidin (violet). Arrows indicate complete ICs in WT and incomplete ICs in *orb2*^{R}. Arrowheads indicate scattered actin cones in mutant testes. Red arrowheads indicate the inverted orientation of scattered actin cones. (D) Quantification of the numbers of testes with IC defects in WT (*n*=86), *orb2*^{R} (*n*=60) and *orb2*^{R}/*orb2*^{36} (*n*=56). (E) DAPI staining for nuclei shows that seminal vesicles in *orb2*^{R} are filled only partially, whereas those in *orb2*^{R}/*orb2*^{36} are empty. (F) Proportions of seminal vesicles with filling defects in WT (*n*=74), *orb2*^{R} (*n*=47) and *orb2*^{R}/*orb2*^{36} (*n*=37). Scale bars: 40 µm (A); 100 µm (C); 15 µm (C, insets); 40 µm (E).

37 (*orb2*-RH). We generated a deletion that removed 32 out of 37 CPE-like elements, and the resultant allele was named *orb2*^{R}. This deletion was downstream of the *orb2*-RB polyadenylation site but included the *orb2*-RC and *orb2*-RD polyadenylation sites. As a result, *orb2*-RC, *orb2*-RD and *orb2*-RH were predicted to all have the same polyadenylation site and contain a total of five CPE-like elements in a 3′UTR of 1269 nt in length.

Although *orb2* has essential functions during meiosis, these functions are not disrupted in *orb2*^{R} and 64-cell spermatid cysts are formed without any visible defects. This finding indicates that the *orb2* 3′UTR is not required for meiosis. By contrast, the 3′UTR is required for spermatid differentiation. The earliest observed defect is in the polarization of the spermatid cyst. In WT cysts, the spermatid nuclei cluster towards the basal side of the cyst. This process is perturbed in *orb2*^{R}, and the nuclei in a subset of mutant cysts remain scattered through the cyst. There are also alterations in the distribution of the βNACtes proteins in these early cysts. Instead of assembling into a series of ordered and evenly spaced longitudinal stripes, the βNACtes stripes in *orb2*^{R} are either disorganized or absent. When *orb2*^{R} is combined with the null allele, *orb2*^{36}, all cysts exhibit these polarization defects. In this context, it should be noted that defects in the early steps of cyst polarization were also observed in testes of males homozygous for the null allele, *orb2*^{36} (Xu et al., 2012, 2014). However, interpreting these polarization defects was complicated because meiosis does not take place in *orb2*^{36} and thus abnormalities in polarization could be an indirect consequence of the meiotic arrest or in difficulties polarizing an abnormal 16-cell cyst. The fact that there are polarization defects in *orb2*^{R} cysts and *orb2*^{R}/*orb2*^{36} cysts where meiosis is unaffected lends support to the idea that *orb2* plays a crucial function at an early point in cyst polarization. The results also implicate the *orb2* 3′UTR in this very early step in spermatid differentiation.

At later stages of cyst differentiation, the 3′UTR deletion also disrupts the localization of *orb2* mRNA and protein near the tips of the elongating flagellar axonemes. Similar localization defects are observed for Boule and for *orb* mRNA and protein. Accompanying these defects in mRNA and protein localization, the morphology of spermatid tails in the region close to the elongating tip is also abnormal. The tail in WT resembles a cylinder with a similar diameter throughout its length. In *orb2*^{R} and *orb2*^{R}/*orb2*^{36}, the tails in the region near the tip are tapered into a point. This altered

Development (2021) 148, dev198788. doi:10.1242/dev.198788

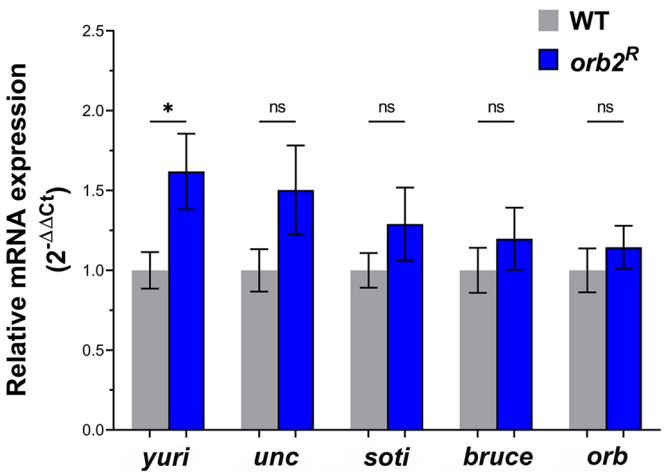

Fig. 9. Expression of spermatogenesis-specific genes in *orb2*^{R} testes. The levels of *yuri*, *unc*, *soti*, *Bruce* and *orb* mRNAs in *orb2*^{R} mutant testes. Data were first normalized to the expression of *Gapdh2* in testes and expressed as the mean fold change [$2^{-\Delta\Delta Ct}$]±s.e.m. in mutant testes relative to control testes (WT and *orb2*^{R} *yuri*, *orb* *n*=9; WT and *orb2*^{R} *soti*, *Bruce* *n*=12; WT and *orb2*^{R} *unc* *n*=10). *P<0.05; ns, not significant.

morphology raises the possibility that the extent of elongation of the individual flagellar axonemes is not uniform within the mutant cysts. If this is the case, it suggests that the localization of Orb2 protein (and mRNA) in a band near the growing tip is likely to be important for ensuring that axonemes lengthen at uniform rate. Although the progressive alterations in chromosome structure that accompany the maturation of the spermatids appear to take place, other steps in the maturation process are defective. These include the coalescence of the spermatid nuclei into a cap-like structure and the assembly and progression of the IC down the flagellar axoneme. Because of these defects, most *orb2*^{R} males are sterile, and the few that are fertile have a significantly reduced number of offspring.

Our results indicate that the *orb2* 3′UTR has important roles in spermatid differentiation, but they also raise several interesting questions. We have found that the levels of *orb2* transcript and protein in *orb2*^{R} are reduced by about 50%. The simplest interpretation of this result is that the presence of intact 3′UTRs is important for *orb2* mRNA stability. However, in view of the sequence organization of the *orb2*^{R} deletion, it is also possible that the reduced mRNA and, consequently, protein levels is due to an inefficient use of the *orb2*-RH polyadenylation sequence. The reduction in the levels of *orb2*^{R} gene products is accompanied by variable and incompletely penetrant effects on spermatogenesis and male fertility. One explanation for these phenotypes is that *orb2* is haploinsufficient for several essential steps in spermatid differentiation and maturation. However, heterozygosity for *orb2*^{36} (an *orb2* deletion) results in an even greater reduction in *orb2* transcripts and protein without any concomitant effect on male fertility. Thus, a more likely explanation for the impairment of spermatogenesis and fertility in *orb2*^{R} is that the deleted 3′UTR sequences are required not only for normal mRNA accumulation but also for *orb2* function. Given that *orb2* transcripts and proteins are not properly localized during flagellar axoneme elongation, a plausible conclusion is that the deleted sequences are needed to facilitate the localization and/or translational regulation of *orb2* transcripts. In *orb2*^{R}, insufficient amounts of Orb2 protein are produced in the cytoplasmic domains where it is required, and this, in turn, affects the localization of other transcripts and proteins (such as Boule and Orb) that have important roles in spermatogenesis.

Although our findings indicate that the deleted 3′UTR sequences are required for full *orb2* activity, the mutant phenotypes are variable and incompletely penetrant. This contrasts with the effects of deletions in the *orb* 3′UTR, which completely disrupts its key functions during oogenesis (Barr et al., 2019). In the case of *orb2*, it is possible that there are other 3′UTR-independent mechanisms that can partially compensate for the defects in *orb2* function resulting from the 3′UTR deletion. It is also possible that this variability reflects the functional properties of this mutant *orb2* gene. In this respect, it is noteworthy that all transcripts produced by the *orb2*^{R} mutant, except *orb2*-RB, are predicted to have a fairly long 3′UTR that retains five CPE-like elements. These five CPEs contain the sequences UUUUUGU and UUUUUGUU, which have been found to be enriched in Orb2-associated transcripts in tissue culture cells (Stepien et al., 2016). Thus, the variable and incompletely penetrant phenotypes may arise because the 3′UTR still retains some functionality.

Taken together, our data show that the 3′UTR of the *orb2* mRNA has a crucial role in the regulation of its localization in spermatids. It implies the existence of an *orb2* self-regulation feedback loop, which is important for male fertility.

MATERIALS AND METHODS

Drosophila stocks

The fly stock expressing Cas9 (*w*^{1118}*; PBac{vas-Cas9}VK00027,* #51324 from Bloomington *Drosophila* Stock Center) was used as WT control. The *orb2*^{36} stock (*w*; PBac{WHr}orb2*^{36}*/TM3, P{GAL4-twi.G}2.3, P{UAS-2xEGFP}AH2.3, Sb*^{1} *Ser*^{1}, #58479 from the Bloomington *Drosophila* Stock Center) was described previously (Xu et al., 2012).

Generation of the *orb2*^{R} allele

Two guide RNAs were used to delete a portion of the *orb2* 3′UTR using the CRISPR/Cas9 system (see Supplementary Materials and Methods for sequences). gRNA sequences were cloned into pU6 vector (pU6-gRNA, Addgene plasmid #53062; a gift from Caixia Gao), and corresponding 1-kbp homology arms were cloned into pHD vector (pHD-DsRed, Addgene plasmid #51434; a gift from Kate O'Connor-Giles). These constructs were injected into the Cas9 fly stock, and dsRed-positive flies were selected. The marker was removed using loxP sites, and the 3′UTR of *orb2*^{R} was sequenced.

Fertility assay

Groups of 20-35 male flies of the WT, *orb2*^{R} and *orb2*^{R}*/orb2*^{36} genotypes were individually crossed with two WT virgin females for 7 days, and then adult flies were removed from the vials. The presence of F1 larvae, pupae and adults in the vials was examined during the next 11 days. The males that were able to mate and produce larvae were regarded as fertile.

Breeding efficiency analysis

For breeding efficiency analysis, 175 WT males, 43 *orb2*^{R} males and 173 *orb2*^{R}*/orb2*^{36} males were individually crossed to WT virgin female flies for 7 days. The adult flies were then removed, and the numbers of offspring from each individual male were estimated.

Viability assay

The viability test was based on Mendelian inheritance in the offspring of *orb2*^{R} and *orb2*^{R}*/orb2*^{36} alleles. For *orb2*^{R}, individual *orb2*^{R}*/TM3 Ser* male and female flies were crossed with each other for 7 days; for *orb2*^{R}*/orb2*^{36}, crosses were made between individual *orb2*^{36}*/TM3 Ser, Sb* males and *orb2*^{R}*/TM3 Ser* females. After the next 2 weeks, the phenotypic ratio in the offspring was evaluated by chi-square analysis.

Development (2021) 148, dev198788. doi:10.1242/dev.198788

Antibodies

The antibodies used were as follows: mouse anti-Orb2 (4G8) at 1:100 for western blotting, mouse anti-Orb2 (4G8 and 2D11) at 1:25 and mouse anti-Orb (6H4) at 1:30 for whole testis staining. These antibodies were deposited to the Developmental Studies Hybridoma Bank (DSHB) by P. Schedl. Mouse anti-cyclin A (A12) antibody (used at 1:500) was deposited to the DSHB by C. F. Lehner; mouse anti-cyclin B (F2F4) antibody (used at 1:500) was deposited to the DSHB by P. H. O'Farrell. Rabbit anti-βNACtes (used at 1:300) was a gift of Dr G. L. Kogan (Institute of Molecular Genetics, National Research Centre Kurchatov Institute, Moscow, Russia). Rabbit anti-Bol (used at 1:1500) was a gift from Steven Wasserman (University of California San Diego, La Jolla, CA, USA). Secondary antibodies were goat anti-mouse IgG conjugated with Alexa 488 (A-11001) or 555 (A-21422) and goat anti-rabbit IgG conjugated with Alexa 555 (A-21428) (Invitrogen). Alexa 633-phalloidin (A22284) at 1:300 (Thermo Fisher Scientific) was used for actin staining in whole mounts of testes. Secondary goat anti-mouse IgG HRP-conjugated antibody (115-035-174) (Jackson ImmunoResearch) was used for western blotting at 1:2000.

Whole-mount immunostaining

Testes from 1- to 3-day-old males were dissected in PBST (0.1% Tween-20 in 1× PBS), fixed in 4% paraformaldehyde for 20 min, washed three times with PBST (here and below, each wash for 5 min), and then passed through an ascending-descending methanol wash series (30%, 50%, 70%, 100%, 70%, 50%, 30% in 1×PBS). The testes were then washed twice with PBST and incubated in PBSTX (0.1% Tween-20 and 0.3% Triton X-100 in 1×PBS) with 5% normal goat serum (Life Technologies) at room temperature for at least 1 h. This was followed by overnight incubation with primary antibody and, after washing three times with PBSTX, with secondary antibody at room temperature for at least 2 h. After final washing three times with PBSTX, the preparations were mounted on slides in VECTASHIELD mounting medium with DAPI (Vector Laboratories).

Fluorescence *in situ* hybridization (FISH)

Quasar 670-conjugated *orb2* and *orb* FISH probes were from LGC Biosearch Technologies (Xu et al., 2014). Testes were taken from young male flies that were fed yeast paste for 2-3 days. They were dissected in 1×PBS, fixed in 4% paraformaldehyde for 30 min, rinsed four times with PBST, dehydrated through an ascending methanol series, and stored in 100% methanol at −20°C for 10 min. After rehydration in PBST, the testes were additionally rinsed four times with PBST, then transferred to wash buffer (4×SSC, 35% formamide, 0.1% Tween-20) for 15 min at 37°C. This was followed by incubation with the FISH probes overnight at 37°C in hybridization buffer (10% dextran sulfate, 0.01% salmon sperm single-strand DNA, 1% vanadyl ribonucleoside, 0.2% bovine serum albumin, 4×SSC, 0.1% Tween-20, and 35% formamide). The resulting preparations were washed twice with wash buffer, 1 h each, at 37°C and mounted in Aqua-Poly/Mount (Polysciences).

Microscopy

Stained preparations were scanned and imaged under an LSM 510 META confocal laser scanning microscope (Carl Zeiss) in multichannel mode using 63× or 40× oil objective lenses and 10× air objective lens (numerical aperture 1.4). Images with a frame size of 1024×1024 pixels and a *z* resolution of 1 µm were taken at a scan speed of 7, in four replicates, and imported into Imaris 5.0.1 (Bitplane) and Adobe Photoshop for subsequent processing.

RNA isolation, reverse transcription, and qPCR

Testes of 1- to 3-day-old male flies were dissected in cold 1× PBS. Total RNA was isolated from 25 pairs of testes using TRIzol (Life Technologies) according to the manufacturer's protocol, treated with DNase (TURBO DNA-free kit, Thermo Fisher Scientific), and reverse transcribed into cDNA. The amount of the transcripts was estimated using gene-specific primers (see Supplementary Materials and Methods). RT-qPCR (reverse transcription-quantitative polymerase chain reaction) for each sample was performed in technical triplicate. The data presented correspond to the mean of $2^{-\Delta\Delta Ct}$ from at least ten independent experiments.

Semi-quantitative western blotting

Testes of 1- to 3-day-old male flies were dissected in cold 1× PBS and immediately transferred to lysis buffer [10 mM HEPES, pH 7.4, 100 mM KCl, 5 mM $MgCl_2$, 0.5% NP-40, 1 mM DDT, 1×cOmplete Protease Inhibitor Cocktail (Roche), 100 µM PMSF]. Total protein lysates were prepared from 25 pairs of testes and loaded in equal dilution series (5, 10 and 20 µg) onto a precast stain-free PAAG gel (Bio-Rad). After electrophoresis, the gel was visualized in a ChemiDoc system (Bio-Rad) to evaluate protein concentrations and perform normalization against the total protein level. The proteins from the gel were blotted onto a PVDF membrane, which was incubated with primary antibodies, secondary HRP-conjugated antibodies, and the Super Signal Western Femto substrate (Thermo Fisher Scientific). The induced chemiluminescence was measured with a ChemiDoc visualization system.

Quantification and statistical analysis

orb2 mRNA and protein enrichment was calculated using average intensity projections of the growing end of spermatid cysts (Fig. 5E). First, the mean fluorescence intensity of the growing tip of the flagellar axoneme was determined by averaging several *z*-stacks in the three areas of interest. The mean fluorescence intensity in spermatocytes was determined in the same way. Then, the mean fluorescence intensity of each area of interest within a spermatid was divided by the mean fluorescence intensity of spermatocytes for each testis. These ratios are shown as box plots. Imaris software was used to quantify the fluorescence signal of *orb2* mRNA and Orb2 protein.

Experimental data were processed statistically with GraphPad Prism software. The statistical significance of the observed differences was estimated by unpaired two-tailed *t*-test (Figs 3A and 5E). Mendelian inheritance in the offspring was analyzed using the nonparametric chi-square method. Variable values for each group are presented as the mean ±s.d. or ±s.e.m. For all panels, *P<0.05, **P<0.005, ***P<0.0005, ****P<0.0001; ns, not significant.

Acknowledgements

The authors are grateful to the Center for Precision Genome Editing and Genetic Technologies for Biomedicine of IGB RAS for mRNA and protein quantification, the Core Facilities Center of IGB RAS, and the IMG RAS Core Facility 'Center of Cell and Gene Technologies' for providing the equipment for microscopy.

Competing interests

The authors declare no competing or financial interests.

Author contributions

Conceptualization: P.S., Y.V.S.; Methodology: P.S., Y.V.S., J.B.; Formal analysis: R.G.; Investigation: R.G., E.N.K., L.V.O., A.A.K., J.B., M.Z.; Data curation: R.G., L.V.O., A.A.K., P.S., Y.V.S.; Writing - original draft: R.G., E.N.K., P.S., Y.V.S.; Writing - review & editing: K.V.Y., M.Z.; Visualization: R.G., K.V.Y.; Supervision: Y.V.S.; Project administration: Y.V.S.; Funding acquisition: M.Z.

Funding

This study was supported by the Russian Science Foundation (18-74-10051 to M.Z., experimental work) and a National Institutes of Health (R35GM126975 to P.S., conceptualization and manuscript preparation). Deposited in PMC for release after 12 months.

Peer review history

The peer review history is available online at https://journals.biologists.com/dev/article-lookup/doi/10.1242/dev.198788

References

Baker, J. D., Adhikarakunnathu, S. and Kernan, M. J. (2004). Mechanosensory-defective, male-sterile unc mutants identify a novel basal body protein required for ciliogenesis in *Drosophila*. *Development* **131**, 3411-3422. doi:10.1242/dev.01229

Barr, J., Yakovlev, K. V., Shidlovskii, Y. and Schedl, P. (2016). Establishing and maintaining cell polarity with mRNA localization in *Drosophila*. *BioEssays* **38**, 244-253. doi:10.1002/bies.201500088

Barr, J., Gilmutdinov, R., Wang, L., Shidlovskii, Y. and Schedl, P. (2019). The *Drosophila* CPEB protein Orb specifies oocyte fate by a 3'UTR-dependent autoregulatory loop. *Genetics* **213**, 1431-1446. doi:10.1534/genetics.119.302687

Barreau, C., Benson, E., Gudmannsdottir, E., Newton, F. and White-Cooper, H. (2008). Post-meiotic transcription in *Drosophila* testes. *Development* **135**, 1897-1902. doi:10.1242/dev.021949

Besse, F. and Ephrussi, A. (2008). Translational control of localized mRNAs: restricting protein synthesis in space and time. *Nat. Rev. Mol. Cell Biol.* **9**, 971-980. doi:10.1038/nrm2548
Castagnetti, S. and Ephrussi, A. (2003). Orb and a long poly(A) tail are required for efficient oskartranslation at the posterior pole of the *Drosophila* oocyte. *Development* **130**, 835-843. doi:10.1242/dev.00309
Chang, J. S., Tan, L. and Schedl, P. (1999). The *Drosophila* CPEB homolog, orb, is required for oskar protein expression in oocytes. *Dev. Biol.* **215**, 91-106. doi:10.1006/dbio.1999.9444
Chang, J. S., Tan, L., Wolf, M. R. and Schedl, P. (2001). Functioning of the *Drosophila* orb gene in gurken mRNA localization and translation. *Development* **128**, 3169-3177. doi:10.1242/dev.128.16.3169
Cheng, M. H., Maines, J. Z. and Wasserman, S. A. (1998). Biphasic subcellular localization of the DAZL-related protein boule in *Drosophila* spermatogenesis. *Dev. Biol.* **204**, 567-576. doi:10.1006/dbio.1998.9098
Christerson, L. B. and McKearin, D. M. (1994). orb is required for anteroposterior and dorsoventral patterning during *Drosophila* oogenesis. *Genes Dev.* **8**, 614-628. doi:10.1101/gad.8.5.614
Fabian, L. and Brill, J. A. (2012). *Drosophila* spermiogenesis: big things come from little packages. *Spermatogenesis* **2**, 197-212. doi:10.4161/spmg.21798
Fabrizio, J. J., Hime, G., Lemmon, S. K. and Bazinet, C. (1998). Genetic dissection of sperm individualization in *Drosophila* melanogaster. *Development* **125**, 1833-1843. doi:10.1242/dev.125.10.1833
Groppo, R. and Richter, J. D. (2011). CPEB control of NF-κB nuclear localization and interleukin-6 production mediates cellular senescence. *Mol. Cell Biol.* **31**, 2707-2714. doi:10.1128/MCB.05133-11
Hafer, N., Xu, S., Bhat, K. M. and Schedl, P. (2011). The *Drosophila* CPEB protein Orb2 has a novel expression pattern and is important for asymmetric cell division and nervous system function. *Genetics* **189**, 907-921. doi:10.1534/genetics.110.123646
Hervás, R., Li, L., Majumdar, A., Fernández-Ramirez Mdel, C., Unruh, J. R., Slaughter, B. D., Galera-Prat, A., Santana, E., Suzuki, M., Nagai, Y. et al. (2016). Molecular basis of Orb2 amyloidogenesis and blockade of memory consolidation. *PLoS Biol.* **14**, e1002361. doi:10.1371/journal.pbio.1002361
Hervas, R., Rau, M. J., Park, Y., Zhang, W., Murzin, A. G., Fitzpatrick, J. A. J., Scheres, S. H. W. and Si, K. (2020). Cryo-EM structure of a neuronal functional amyloid implicated in memory persistence in *Drosophila*. *Science* **367**, 1230-1234. doi:10.1126/science.aba3526
Hochegger, H., Klotzbücher, A., Kirk, J., Howell, M., le Guellec, K., Fletcher, K., Duncan, T., Sohail, M. and Hunt, T. (2001). New B-type cyclin synthesis is required between meiosis I and II during Xenopus oocyte maturation. *Development* **128**, 3795-3807. doi:10.1242/dev.128.19.3795
Igea, A. and Méndez, R. (2010). Meiosis requires a translational positive loop where CPEB1 ensues its replacement by CPEB4. *EMBO J.* **29**, 2182-2193. doi:10.1038/emboj.2010.111
Ivshina, M., Lasko, P. and Richter, J. D. (2014). Cytoplasmic polyadenylation element binding proteins in development, health, and disease. *Annu. Rev. Cell Dev. Biol.* **30**, 393-415. doi:10.1146/annurev-cellbio-101011-155831
Kaplan, Y., Gibbs-Bar, L., Kalifa, Y., Feinstein-Rotkopf, Y. and Arama, E. (2010). Gradients of a ubiquitin E3 ligase inhibitor and a caspase inhibitor determine differentiation or death in spermatids. *Dev. Cell* **19**, 160-173. doi:10.1016/j.devcel.2010.06.009
Khan, M. R., Li, L., Pérez-Sánchez, C., Saraf, A., Florens, L., Slaughter, B. D., Unruh, J. R. and Si, K. (2015). Amyloidogenic oligomerization transforms *Drosophila* Orb2 from a translation repressor to an activator. *Cell* **163**, 1468-1483. doi:10.1016/j.cell.2015.11.020
Kogan, G. L., Akulenko, N. V., Abramov, Y. A., Sokolova, O. A., Fefelova, E. A. and Gvozdev, V. A. (2017). Nascent polypeptide-associated complex as tissue-specific cofactor during germinal cell differentiation in *Drosophila* testes. *Mol. Biol.* **51**, 596-601 doi:10.1134/S0026893317040112
Kronja, I. and Orr-Weaver, T. L. (2011). Translational regulation of the cell cycle: when, where, how and why? *Philos. Trans. R. Soc. B Biol. Sci.* **366**, 3638-3652. doi:10.1098/rstb.2011.0084
Krüttner, S., Stepien, B., Noordermeer, J. N., Mommaas, M. A., Mechtler, K., Dickson, B. J. and Keleman, K. (2012). *Drosophila* CPEB Orb2A mediates memory independent of Its RNA-binding domain. *Neuron* **76**, 383-395. doi:10.1016/j.neuron.2012.08.028
Krüttner, S., Traunmüller, L., Dag, U., Jandrasits, K., Stepien, B., Iyer, N., Fradkin, L. G., Noordermeer, J. N., Mensh, B. D. and Keleman, K. (2015). Synaptic Orb2A bridges memory acquisition and late memory consolidation in *Drosophila*. *Cell Rep.* **11**, 1953-1965. doi:10.1016/j.celrep.2015.05.037
Lantz, V., Ambrosio, L. and Schedl, P. (1992). The Drosophila orb gene is predicted to encode sex-specific germline RNA-binding proteins and has localized transcripts in ovaries and early embryos. *Development* **115**, 75-88. doi:10.1242/dev.115.1.75
Lasko, P. (2012). mRNA localization and translational control in *Drosophila* oogenesis. *Cold Spring Harb. Perspect. Biol.* **4**, a012294. doi:10.1101/cshperspect.a012294
Martin, K. C. and Ephrussi, A. (2009). mRNA localization: gene expression in the spatial dimension. *Cell* **136**, 719-730. doi:10.1016/j.cell.2009.01.044
Mastushita-Sakai, T., White-Grindley, E., Samuelson, J., Seidel, C. and Si, K. (2010). Drosophila Orb2 targets genes involved in neuronal growth, synapse formation, and protein turnover. *Proc. Natl. Acad. Sci. USA* **107**, 11987-11992. doi:10.1073/pnas.1004433107
McCaffrey, L. M. and Macara, I. G. (2009). Widely conserved signaling pathways in the establishment of cell polarity. *Cold Spring Harb. Perspect. Biol.* **1**, a001370. doi:10.1101/cshperspect.a001370
Nelson, W. J. (2003). Adaptation of core mechanisms to generate cell polarity. *Nature* **422**, 766-774. doi:10.1038/nature01602
Noguchi, T. and Miller, K. G. (2003). A role for actin dynamics in individualization during spermatogenesis in *Drosophila* melanogaster. *Development* **130**, 1805-1816. doi:10.1242/dev.00406
O'Donnell, L. (2014). Mechanisms of spermiogenesis and spermiation and how they are disturbed. *Spermatogenesis* **4**, e979623. doi:10.4161/21565562.2014.979623
Rathke, C., Baarends, W. M., Jayaramaiah-Raja, S., Bartkuhn, M., Renkawitz, R. and Renkawitz-Pohl, R. (2007). Transition from a nucleosome-based to a protamine-based chromatin configuration during spermiogenesis in *Drosophila*. *J. Cell Sci.* **120**, 1689-1700. doi:10.1242/jcs.004663
Richter, J. D. (2007). CPEB: a life in translation. *Trends Biochem. Sci.* **32**, 279-285. doi:10.1016/j.tibs.2007.04.004
Sarkissian, M., Mendez, R. and Richter, J. D. (2004). Progesterone and insulin stimulation of CPEB-dependent polyadenylation is regulated by Aurora A and glycogen synthase kinase-3. *Genes Dev.* **18**, 48-61. doi:10.1101/gad.1136004
St Johnston, D. (2005). Moving messages: the intracellular localization of mRNAs. *Nat. Rev. Mol. Cell Biol.* **6**, 363-375. doi:10.1038/nrm1643
Stepien, B. K., Oppitz, C., Gerlach, D., Dag, U., Novatchkova, M., Krüttner, S., Stark, A. and Keleman, K. (2016). RNA-binding profiles of *Drosophila* CPEB proteins Orb and Orb2. *Proc. Natl. Acad. Sci. USA* **113**, E7030-E7038. doi:10.1073/pnas.1603715113
Tan, L., Chang, J. S., Costa, A. and Schedl, P. (2001). An autoregulatory feedback loop directs the localized expression of the *Drosophila* CPEB protein Orb in the developing oocyte. *Development* **128**, 1159-1169. doi:10.1242/dev.128.7.1159
Texada, M. J., Simonette, R. A., Johnson, C. B., Deery, W. J. and Beckingham, K. M. (2008). Yuri gagarin is required for actin, tubulin and basal body functions in *Drosophila* spermatogenesis. *J. Cell Sci.* **121**, 1926-1936. doi:10.1242/jcs.026559
Tokuyasu, K. T. (1974). Dynamics of spermiogenesis in *Drosophila* melanogaster: III. Relation between axoneme and mitochondrial derivatives. *Exp. Cell Res.* **84**, 239-250. doi:10.1016/0014-4827(74)90402-9
Tokuyasu, K. T. (1975). Dynamics of spermiogenesis in *Drosophila* melanogaster: V. Head-tail alignment. *J. Ultrastr. Res.* **50**, 117-129. doi:10.1016/S0022-5320(75)90013-1
Tokuyasu, K. T., Peacock, W. J. and Hardy, R. W. (1972). Dynamics of spermiogenesis in *Drosophila* melanogaster. II. Coiling process. *Z. Zellforsch. Mikrosk. Anat.* **127**, 492-525. doi:10.1007/BF00306868
Xu, S., Hafer, N., Agunwamba, B. and Schedl, P. (2012). The CPEB protein Orb2 has multiple functions during spermatogenesis in *Drosophila* melanogaster. *PLoS Genet.* **8**, e1003079. doi:10.1371/journal.pgen.1003079
Xu, S., Tyagi, S. and Schedl, P. (2014). Spermatid cyst polarization in *Drosophila* depends upon apkc and the CPEB family translational regulator orb2. *PLoS Genet.* **10**, e1004380. doi:10.1371/journal.pgen.1004380